Copy No. 34

DEFENCE R&D DÉFENSE

NON-LOCAL BOUNDARY CONDITIONS FOR HIGH-ORDER PE MODELS WITH APPLICATION TO SCATTERING FROM A ROUGH SURFACE

G.H. Brooke & D.J. Thomson

DEFENCE RESEARCH ESTABLISHMENT ATLANTIC

Technical Memorandum

DREA TM 1999-121

August 1999

Défense nationale National Defence

Canada

National Defence
Research and Development Branch

Défense nationale
Bureau de recherche et développement

DREA TM 1999/121

NON-LOCAL BOUNDARY CONDITIONS FOR HIGH-ORDER PE MODELS WITH APPLICATION TO SCATTERING FROM A ROUGH SURFACE

G.H. Brooke & D.J. Thomson

DEFENCE RESEARCH ESTABLISHMENT ATLANTIC
PO Box 1012 Dartmouth
Nova Scotia, Canada
B2Y 3Z7

Approved by

J.S. Kennedy
Head, Underwater Acoustics

August 1999

TECHNICAL MEMORANDUM

Prepared by

Defence Research Establishment Atlantic

Centre de Recherches pour la Défense Atlantique

Canada

Abstract

Numerical PE (parabolic equation) solvers for underwater sound propagation usually approximate the subbottom radiation condition by appending an absorbing layer to the computational mesh. An alternative procedure uses a non-local boundary condition (NLBC) applied along (or below) the sea-bottom interface that *exactly* transforms the semi-infinite PE configuration into an equivalent bounded domain. In this paper, we analyze NLBC's that are expressed in terms of plane-wave reflection coefficients and describe their implementation in the context of higher-order Padé-based PE algorithms. In particular, we develop non-local boundary conditions to account for the coherent losses due to scattering by a statistically-rough sea surface. Several numerical examples are presented to illustrate the numerical implementation of NLBC's for higher-order PE's.

Résumé

Les solutionneurs d'équations paraboliques (EP) numériques pour la propagation du son sous l'eau établissent habituellement approximativement la condition de rayonnement sous le plancher océanique en ajoutant une couche absorbante à la maille de calcul. Une autre procédure consiste à établir une condition frontière extérieure (CFE) que l'on applique le long de l'interface mer/plancher océanique (ou sous cette dernière) et qui transforme exactement la configuration EP à demi infinie en un domaine limité équivalent. Dans le présent document, nous analysons les CFE qui sont exprimées en termes de coefficients de réflexion d'ondes planes et nous décrivons leur mise en application dans le contexte d'algorithmes EP basés sur Padé et de degré élevé. Plus particulièrement, nous élaborons des conditions frontières extérieures pour tenir compte des pertes cohérentes imputables à la diffusion par une surface de mer estimée statistiquement. Plusieurs exemples numériques sont présentés afin d'illustrer la mise en application numérique des CFE pour les EP de degré élevé.

102-02829/

DREA TM 1999–121

Non-Local Boundary Conditions for High-order PE Models with Application to Scattering from a Rough Surface

by

G.H. Brooke & D.J. Thomson

Executive Summary

Introduction

Parabolic equation (PE) solvers for underwater sound applications usually approximate the downgoing radiation condition numerically by appending an absorbing layer to base of the computational grid. In contrast, non-local boundary conditions (NLBC's) can be introduced along (or below) the sea-bottom interface that *exactly* transform the original semi-infinite PE problem to an equivalent one in a bounded domain. Here we analyze NLBC's in terms of plane-wave reflection coefficients and describe their implementation in the context of high-order, multi-term Padé and split-step Padé PE algorithms.

Principal Results

New non-local boundary conditions are developed for the Tappert, Claerbout and Exact PE's that account for the coherent losses due to a statistically-rough sea surface. We establish that these rough-surface NLBC's based on single-term PE's can be combined with corresponding NLBC's for a fluid bottom and incorporated into high-order, multi-term, Padé-based PEs to yield accurate numerical solutions to far-field acoustic propagation.

Significance of the Results

In addition to reducing the size of the computational domain, NLBC's based on single-term PE's are readily implemented in existing high-order, Padé-based parabolic equation codes and provide an efficient method of accommodating the coherent scattering losses due to a rough surface.

Future Plans

For high-frequency propagation over a lossy bottom, our numerical results indicate that the use of NLBC's can compromise the larger range step-size capability usually associated with the split-step Padé PE algorithm. We believe that our present NLBC routines, which are based on a procedure for computing integrals involving Bessel functions with complex arguments, need further improvement.

Contents

Abstract i

Executive Summary iii

Table of Contents v

List of Figures v

1 Introduction 1

2 PE Algorithms 2

3 Non-Local Boundary Conditions 5
- 3.1 Vertical Wavenumbers for PE's 6
- 3.2 A Rough Free Surface 8
- 3.3 Fluid Half-space 9
- 3.4 Discussion 10

4 Numerical Examples 11
- 4.1 Example 1: Bucker waveguide 11
- 4.2 Example 2: Pekeris waveguide 12
- 4.3 Example 3: ASA Wedge 14

5 Summary 16

References 16

Appendices 21

A Intermediate PE Fields 21

B NLBC Implementation 22

List of Figures

1 Transmission loss comparison for the Bucker waveguide. 11
2 Transmission loss comparison for the Bucker waveguide. 12
3 Transmission loss comparison for the Pekeris waveguide. 13
4 Transmission loss comparison for the Pekeris waveguide. 13
5 Transmission loss comparison for the ASA wedge. 15
6 Transmission loss comparison for the ASA wedge. 15

1 Introduction

Long range propagation of underwater sound is strongly influenced by interaction with top and bottom ocean boundaries. In deep water, this interaction affects predominantly the high-angle energy and occurs near the ocean surface, e.g., a wind-driven sea surface or the rough underside of multi-year Arctic pack ice. Bottom losses usually limit sea-floor interactions to short ranges in deep water. In contrast, low-frequency sound propagating in shallow water interacts significantly with both boundaries and, consequently, boundary effects are much more prevalent even for low-angle propagation. To complicate matters, the ocean boundaries are often range-dependent and, at some scale, rough. Since popular source localization schemes such as matched field processing [1] rely on correlating acoustic predictions with measured array data, it is important to properly and efficiently model the coherent sound field.

In order to fully characterize these boundary interactions, a detailed specification of the material properties at reflecting interfaces is required. In practice, these data can be logistically difficult to obtain and often lack sufficient detail to meet fully the needs of most models. Moreover, field measurements sometimes infer a related parameter (e.g., the reflection coefficient) and may not describe the physical characteristics of the medium directly. Consequently, propagation model enhancement and development is strategic in the attempt to provide a reasonable accounting of the interaction of acoustic energy with the ocean boundaries, and furthermore, to develop useful advanced signal processing schemes. Several numerical models [2, 3] are currently used to calculate the transmission of sound underwater—the selection of a particular model depends on the problem at hand. Here, we choose to concentrate on the parabolic equation (PE) model since it has application to both shallow and deep water and, in particular, to range-dependent waveguides.

PE propagation models have undergone extensive improvements in recent years [3, pp. 343–412]. As attention has shifted to shallow water, the split-step Fourier method [4, 5, 6], well-suited to narrow-angle deep-water problems, has been been complemented by a suite of finite-difference methods [7, 8, 9]. Modern finite-difference algorithms have been developed for the PE to address specific issues such as accuracy [10, 11, 12], energy-conservation [13], and efficiency [14]. Recent models are also capable of treating complicated waveguide effects such as elasticity [15, 16, 17], backscatter [18, 19, 20] and porosity [21, 22, 23]. In this paper we report on two incremental but important enhancements to finite-difference PE models. Specifically, we introduce new non-local boundary conditions (NLBC's) that account approximately for the coherent effects of a rough ocean surface. Combined with previously developed NLBC's that incorporate the interaction of sound with a fluid half-space, we then apply these boundary conditions within the context of high-order Padé [11] and split-step Padé PE [14] algorithms.

In previous work, non-local boundary conditions have been introduced that allow the vertical extent of the computational grid to be terminated *exactly* [24, p. 83], [25, 26, 27, 28, 29, 30, 31, 32, 33, 34, 35].Of course, the efficiency gain obtained by reducing the number of depth grid points is constrained somewhat by overhead incurred in updating the boundary condition after each range step. The derivation of a non-local boundary condition hinges on *a priori* knowledge of the depth-dependent behaviour of the field in a certain portion of the waveguide. For example, if the lowermost half-space is taken to be homogeneous, then the

analytic form of the associated field is known and can be accounted for using an impedance boundary condition along the boundary interface. This property still holds in cases where the square of the refractive index in the terminating half-space varies linearly with depth [30, 32]. In principle, if the surface impedance function (or equivalently the reflection coefficient) is known as a function of angle, then a non-local boundary condition can be used to account exactly for the effects of any layered inhomogeneous half-space. To date, NLBC's have only been implemented numerically for first-order PE algorithms—the Tappert (Standard) and the Claerbout PE's. Here we extend the application to include higher-order Padé and split-step Padé PE's. Furthermore, we utilize the fact that the non-local conditions can be cast in terms of the reflection coefficient to derive approximate NLBC's for a rough zero-mean Gaussian surface. In particular, we demonstrate the application of the modified high-order PE algorithms in an environment where both the rough surface and a penetrable bottom are treated in the context of non-local boundary conditions. We also illustrate the application of NLBC's for a range-dependent waveguide.

In what follows, we present relevant mathematical analysis associated with the application of non-local boundary conditions to higher-order parabolic equation approximations. We begin with a brief overview of high-order finite-difference PE algorithms based on Padé expansions. Next, we examine the relationships between the vertical wavenumbers that are associated with different PE algorithms—these spectral connections provide the framework for our subsequent analysis. The important fact that the boundary conditions satisfied by the *total* PE field also apply, identically, to the *intermediate* fields associated with higher-order methods is established in Appendix A. To circumvent the complicated numerical implementations implied by these higher-order algorithms, we exploit the spectral relationship between vertical wavenumbers to use simpler first-order NLBC's in conjunction with the high-order propagators. For example, we derive an approximate non-local rough-surface boundary condition based on the Claerbout PE approximation (a first order method) and apply it within the context of a high-order PE algorithm. NLBC relationships based on the Tappert PE approximation and an Exact PE formulation [28] are also presented. The numerical approximations that are used to implement the non-local boundary conditions are developed in Appendix B. Finally, we present several numerical test case results that illustrate the performance obtained with the enhanced PE algorithms.

2 PE Algorithms

Consider a range-independent acoustic medium, bounded above by a free surface at $z = 0$, with a sound speed profile that supports long range propagation (as $r \to \infty$) in the upper part of the waveguide. For $r > 0$, the pressure $p(r, z)$ due to a harmonic point source located at $(r, z) = (0, z_s)$ with time-dependence $\exp(-i\omega t)$ can be obtained by solving the acoustic Helmholtz equation

$$\frac{1}{r}\frac{\partial}{\partial r}\left(r\frac{\partial p}{\partial r}\right) + \rho\frac{\partial}{\partial z}\left(\rho^{-1}\frac{\partial p}{\partial z}\right) + k_0^2 N^2 p = 0. \tag{2.1}$$

Here k_0 is a reference wavenumber while $\rho(z)$ and $N(z) = n(z)[1 + i\alpha(z)]$ represent the density and the complex refractivity of the stratified medium, respectively. It is convenient to introduce a reduced field $\psi(r, z) = p(r, z)\sqrt{r}\exp(-ik_0 r)$ in which case the far-field ($k_0 r \gg 1$)

form of (2.1) can be factored to produce an outgoing field component that satisfies the one-way or parabolic equation

$$\frac{\partial \psi}{\partial r} = ik_0 \left(-1 + \sqrt{1+X}\right)\psi, \tag{2.2}$$

where X is used to denote the differential operator

$$X = N^2 - 1 + k_0^{-2}\rho \frac{\partial}{\partial z}\left(\rho^{-1}\frac{\partial}{\partial z}\right). \tag{2.3}$$

Using (2.2), the Taylor expansion $\psi(r+\Delta r, z) = \exp(\partial_r \Delta r)\psi(r,z)$ yields a marching algorithm that forms the basis for all PE methods, i.e.,

$$\psi(r+\Delta r, z) = \exp\left(-i\delta + i\delta\sqrt{1+X}\right)\psi(r,z), \tag{2.4}$$

where we have set $\delta = k_0 \Delta r$. There are many numerical approaches currently available for solving (2.4) that differ only in the treatment used to approximate the square-root operator. Most finite-difference PE methods discretize the waveguide onto an equi-spaced grid of points in depth and range with spacings Δz and Δr, respectively. Equation (2.4) dictates how the PE field is to be advanced step-by-step in range. Depending on the type, accuracy, and efficiency of PE method desired, specific rational-linear expansions are used to approximate the square-root operator. This procedure exposes the differential operator X in a way that can be handled numerically using a centred-difference representation in the vertical coordinate z (suitably modified to accommodate the density variations).

Basically, two types of Padé expansions are employed in the solution of (2.4). The first involves a rational-linear or Padé expansion of the square-root operator directly as

$$-1 + \sqrt{1+X} \approx \sum_{m=1}^{M} \frac{a_m X}{1 + b_m X}, \tag{2.5}$$

where the real-valued Padé coefficients a_m and b_m are given by

$$a_m = \frac{2}{2M+1}\sin^2\frac{m\pi}{2M+1}, \quad b_m = \cos^2\frac{m\pi}{2M+1}. \tag{2.6}$$

Equation (2.5) can be substituted into (2.4) and leads to a numerical PE solution based on the implicit finite-difference method [3, 11]. We can write

$$\begin{aligned}\psi(r+\Delta r, z) &= \exp\left(i\delta \sum_{m=1}^{M} \frac{a_m X}{1+b_m X}\right)\psi(r,z) \\ &= \prod_{m=1}^{M} \exp\left(\frac{i\delta a_m X}{1+b_m X}\right)\psi(r,z),\end{aligned} \tag{2.7}$$

which can be solved numerically as a sequence of M first-order systems of the form,

$$\psi_m(r,z) = \exp\left(\frac{i\delta a_m X}{1+b_m X}\right)\psi_{m-1}(r,z), \quad m = 1, 2, \ldots, M \tag{2.8}$$

where $\psi_0(r,z) \equiv \psi(r,z)$ and $\psi_M(r,z) \equiv \psi(r+\Delta r, z)$. For $M \geq 2$, the PE algorithm based on (2.7) is referred to as a high-order Padé PE. For $M = 1$, (2.7) reduces to the Claerbout PE ($a_1 = \frac{1}{2}$ and $b_1 = \frac{1}{4}$). The Tappert PE is obtained by setting $a_1 = \frac{1}{2}$ and $b_1 = 0$. The Crank-Nicolson procedure for solving each first-order problem in (2.8) involves approximating the propagator by a unitary rational-linear form to obtain

$$\left(1 + c_m^- X\right) \psi_m(r,z) = \left(1 + c_m^+ X\right) \psi_{m-1}(r,z), \tag{2.9}$$

where $c_m^{\pm} = b_m \pm \frac{1}{2} i\delta a_m$. Employing a finite-difference representation of X in (2.9) leads to the familiar tri-diagonal matrix problem for advancing the PE field one range step. If $M = 1$, then $\psi_1(r,z) = \psi(r+\Delta r, z)$. For $M > 1$, however, then $\psi_1(r,z)$ becomes the input for the next first-order problem in the sequence, etc. Typically, for a low-frequency shallow water problem, grid sizes of the order of 5 m in range and 1 m in depth are required in order to accurately propagate the PE field. High-angle propagation is accommodated by taking a larger number of Padé terms.

More recently [14], a second type of Pade expansion has been introduced in the solution of (2.4) leading to what is known as the split-step Padé PE method. In this approach, a Padé expansion is carried out on the exponential propagator itself such that

$$\exp\left(-i\delta + i\delta\sqrt{1+X}\,\right) \approx 1 + \sum_{m=1}^{M} \frac{A_m X}{1 + B_m X} \tag{2.10}$$

where $\{A_m, B_m\}$ are different than $\{a_m, b_m\}$ in (2.6) and are necessarily complex-valued. Consequently, (2.4) becomes

$$\psi(r+\Delta r, z) \approx \psi(r,z) + \sum_{m=1}^{M} \frac{A_m X}{1 + B_m X}\, \psi(r,z). \tag{2.11}$$

As before, the operator X is handled numerically using finite differences. Specifically, the solution of (2.11) is obtained by solving M tri-diagonal problems for the intermediate fields, $\psi_m(r,z)$, derived from

$$(1 + B_m X)\, \psi_m(r,z) = A_m X \psi(r,z). \tag{2.12}$$

and then by combining the resultant solutions to form

$$\psi(r+\Delta r, z) = \psi(r,z) + \sum_{m=1}^{M} \psi_m(r,z). \tag{2.13}$$

This procedure advances the PE field one range step. The advantages of the split-step Padé PE over the Padé PE are twofold: (i) the Padé expansion of the propagator allows much larger range steps to be accommodated (by an order of magnitude in some problems), and (ii) the solution of the intermediate problems in (2.12) involve only the known field at the current range step and can be computed in parallel on a multiple-processor machine.

In obtaining the numerical solution for the intermediate fields, i.e., either (2.9) or (2.12), we must truncate the depth grid, top and bottom. In most underwater acoustic applications, the grid is truncated above by a pressure-release ocean surface and below, at a suitably large depth, by a combination of an artificial absorbing layer (to miminize reflections) over a

ficticious free boundary. Clearly, the vertical extent of the computation grid is significant in determining the efficiency of the numerical calculations. This fact makes enhancements in range-step capability like that found in the split-step Padé method very attractive. Similarly, procedures that limit the vertical extent of the computational grid are also important, i.e., non-local boundary conditions. Since the PE method is a marching solution, it is routinely applied to range-dependent media by updating the medium at each range step even though it is derived on the basis of range-independence. As will be demonstrated, non-local boundary conditions are applicable to range-dependent problems provided the boundary condition is applied below any range-varying properties in the waveguide.

3 Non-Local Boundary Conditions

Let the ocean/subbottom waveguide combination in $0 < z < z_b$ overlay the uniform fluid half-space $z > z_b$. Traditional finite-difference PE algorithms incorporate boundary conditions associated with this structure by requiring both the pressure $p \propto \psi$ and the vertical particle velocity $v \propto \rho^{-1}\partial_z\psi$ to be continuous across any horizontal interface $z = d \leq z_b$. Because the half-space $z > z_b$ in the present problem is uniform, the PE field in this region must be downgoing in order to satisfy the radiation condition. A non-local boundary condition that represents the field behaviour in the lower half-space may be applied along $z = z_b$ to eliminate the need for an absorbing layer and grid terminus combination. In this case, the resultant PE algorithm is unchanged within $0 < z < z_b$, although additional calculations are required to compute the contribution of the non-local boundary condition along $z = z_b$.

In this paper we introduce non-local boundary conditions, applied at $z = 0$ (free surface), to model the coherent losses due to a rough surface with zero-mean Gaussian statistics. Moreover, it is our objective to implement these non-local boundary conditions within the context of a high-order split-step Padé PE algorithm. Up to now, non-local boundary conditions have been used to represent the effects of half-spaces (either homogeneous [27, 28, 29] or inhomogeneous [30, 32]). These non-local bottom boundary conditions can be combined with NLBC's that treat surface roughness in a single PE code. Previous analyses have been restricted to the first-order Tappert and Claerbout PE's. Furthermore, since the high-order split-step Padé algorithm involves the definition of intermediate field quantities, we must first establish the boundary conditions satisfied by these fields. The modal analysis presented in Appendix A indicates that the intermediate fields satisfy exactly the same boundary conditions as the total PE field. Thus, for any particular higher-order PE, the boundary conditions for the total field can be applied directly to the intermediate fields. It is also important to point out that a NLBC has been derived for (2.2), which we refer to as the Exact NLBC [28]. To the authors' knowledge, this NLBC has never been implemented numerically. We include the Exact NLBC in our discussions since it is intimately related to NLBC's for all finite-difference PE algorithms. Finally, we make a distinction between the order (i.e., accuracy) of the NLBC and the order of the PE method used to propagate the acoustic field in the interior of the waveguide. In fact, we demonstrate that low-order NLBC's are quite adequate when used with high-order propagators—a useful result since high-order NLBC's require more complicated numerical implementations.

Our analysis will depend on the Laplace transform pair

$$\Psi(s,z) = \int_0^\infty \psi(\tau,z)e^{-s\tau}d\tau, \quad \psi(\tau,z) = \frac{1}{2\pi i}\int_{\varepsilon-i\infty}^{\varepsilon+i\infty} \Psi(s,z)e^{+s\tau}ds. \tag{3.1}$$

where we assume that the necessary conditions on $\psi(0,z)$ are met such that $\partial_\tau^\ell \psi(\tau,z) \Leftrightarrow s^\ell\Psi(s,z)$, $\ell = 1,2,\ldots$ for $0 \le z \le z_b$. In the transform domain, it is convenient in the derivation of a non-local boundary condition to combine the usual conditions of continuity along $z = d$ into the single continuity condition for the impedance,

$$G(s) \equiv \left.\frac{\rho\Psi}{\partial_z\Psi}\right|_{d-0} = \left.\frac{\rho\Psi}{\partial_z\Psi}\right|_{d+0}. \tag{3.2}$$

We also utilize a plane-wave analysis in the vicinity of $z = d$ to derive an equivalent form of (3.2) specified in terms of the plane-wave reflection coefficients, $R^\pm(s)$, where the superscript $\pm$ indicates quantities evaluated at $d \pm 0$. Within a thin uniform layer adjacent to $z = d$, we find

$$G(s) = \frac{\rho^\pm}{\mp i\gamma^\pm(s)}\frac{1+R^\pm(s)}{1-R^\pm(s)}, \tag{3.3}$$

where $\gamma^\pm(s)$ is the vertical wavenumber. Rearranging and taking inverse transforms of (3.2) leads directly to a non-local boundary condition along $z = d$ in the form of a Neumann to Dirichlet (NtD) mapping

$$\psi(\tau,d) = \int_0^\tau \partial_z\psi(\tau-t,d)\underbrace{\frac{1}{2\pi i}\int_{\varepsilon-i\infty}^{\varepsilon+i\infty} G(s)e^{st}ds}_{g(t)}\,dt\,. \tag{3.4}$$

Depending on the particular PE approximations involved, the inner integral $g(t)$ can be obtained analytically so that (3.4) reduces to a single outer integral over the range coordinate t. The ability to carry out this analysis depends on the forms of γ and R for a given problem. In particular, the vertical wavenumber γ is dependent on the specific PE algorithm being implemented and is central to the development of non-local boundary conditions.

3.1 Vertical Wavenumbers for PE's

In this section we derive the vertical wavenumbers that can be associated with various PE approximations. The critical equations are (2.2) for regular Padé PE methods and (2.4) for split-step Padé PE methods. In the transform domain, (2.2) for the regular Padé PE becomes

$$s\Psi(s,z) = ik_0\left(-1+\sqrt{1+X}\right)\Psi(s,z). \tag{3.5}$$

For the Tappert PE, this equation reduces to

$$s\Psi(s,z) = \tfrac{1}{2}ik_0X\Psi(s,z) \equiv \tfrac{1}{2}ik_0\left(N^2(z)-1+k_0^{-2}\frac{\partial^2}{\partial z^2}\right)\Psi(s,z) \tag{3.6}$$

whereupon

$$\left(\frac{\partial^2}{\partial z^2}+\gamma_0^2(s,z)\right)\Psi(s,z) = 0 \tag{3.7}$$

and γ_0^2 is given in closed form as

$$\gamma_0^2(s,z) = k_0^2\left\{N^2(z) - 1 - 2s/ik_0\right\}. \tag{3.8}$$

In a similar manner, we can derive an equivalent expression for the Claerbout PE in the form

$$\begin{aligned}\gamma_1^2(s,z) &= k_0^2\left\{N^2(z) - 1 - (2s/ik_0)\left[1 - s/(2ik_0)\right]^{-1}\right\} \\ &= k_0^2\left\{N^2(z) - 1 - 2s/ik_0 + s^2/k_0^2\right\} + O(s^3).\end{aligned} \tag{3.9}$$

The analysis for higher-order ($M \geq 2$) Pade PE's is straightforward but more involved. We note first that

$$\begin{aligned}-1 + \sqrt{1+X} &\approx \sum_{m=1}^{M} \frac{a_m X}{1 + b_m X} \\ &= c_1 X + c_2 X^2 + c_3 X^3 + \cdots + c_{2M} X^{2M} + \cdots\end{aligned} \tag{3.10}$$

Expanding the LHS of (3.10) in a power series in X and equating like powers of X on both sides of the equation leads to the first few sums

$$\begin{aligned} c_1 &= \textstyle\sum_{m=1}^{M} a_m = \frac{1}{2}\,, & c_2 &= -\textstyle\sum_{m=1}^{M} a_m b_m = -\frac{1}{8}\,, \\ c_3 &= \textstyle\sum_{m=1}^{M} a_m b_m^2 = \frac{1}{16}\,, & c_4 &= -\textstyle\sum_{m=1}^{M} a_m b_m^3 = -\frac{5}{128}\,, \ \cdots \end{aligned} \tag{3.11}$$

Substituting (3.10) and (3.11) in (3.5) gives

$$s\Psi(s,z) = ik_0\left(\tfrac{1}{2}X - \tfrac{1}{8}X^2 + \tfrac{1}{16}X^3 - \tfrac{5}{128}X^4 + \cdots\right)\Psi(s,z). \tag{3.12}$$

The series in (3.12) can be reverted to yield [36, p. 16]

$$X = 2s/ik_0 - s^2/k_0^2 + O\left(s^{2M+1}\right), \tag{3.13}$$

from which an expression for the vertical wavenumber associated with the M-th order Padé approximation can be obtained in the form

$$\gamma_M^2(s,z) = k_0^2\left\{N^2(z) - 1 - 2s/ik_0 + s^2/k_0^2\right\} + O\left(s^{2M+1}\right). \tag{3.14}$$

The vertical wavenumber for the Exact PE also derives from (3.5) but involves applying the operator $ik_0\sqrt{1+X}$ to both sides and then substituting from (3.5) to obtain

$$\begin{aligned}\gamma^2(s,z) &= k_0^2\left\{N^2(z) - 1 - (2s/ik_0)(1 - is/2k_0)\right\} \\ &= k_0^2\left\{N^2(z) - 1 - 2s/ik_0 + s^2/k_0^2\right\}.\end{aligned} \tag{3.15}$$

For the split-step Padé PE method, the vertical wavenumbers derive from the transform of (2.4) which can be put in the form

$$\exp(s\Delta r)\,\Psi(s,z) = \exp\left(-i\delta + i\delta\sqrt{1+X}\right)\Psi(s,z). \tag{3.16}$$

Using (2.10) we have

$$-1+\exp\left(-i\delta+i\delta\sqrt{1+X}\right)\approx\sum_{m=1}^{M}\frac{A_mX}{1+B_mX}$$
$$=C_1X+C_2X^2+C_3X^3+\cdots+C_{2M}X^{2M}+\cdots \quad (3.17)$$

where the first few coefficients are related by

$$\begin{array}{lll} C_1= & \sum_{m=1}^{M}A_m & =\frac{1}{2}i\delta, \\ C_2= & \sum_{m=1}^{M}A_mB_m & =-\frac{1}{8}\delta^2-\frac{1}{8}i\delta, \\ C_3= & \sum_{m=1}^{M}A_mB_m^2 & =-\frac{1}{48}i\delta^3+\frac{1}{16}\delta^2+\frac{1}{16}i\delta, \\ C_4= & \sum_{m=1}^{M}A_mB_m^3 & =\frac{1}{384}\delta^4+\frac{1}{64}i\delta^3-\frac{5}{128}\delta^2-\frac{5}{128}i\delta,\ \cdots \end{array} \quad (3.18)$$

Setting $E(s)=-1+\exp(s\Delta r)=s\Delta r+\frac{1}{2}s^2\Delta r^2+\cdots$, the series obtained by combining (3.16)–(3.18) can be reverted to yield

$$X=C_1^{-1}E-C_2C_1^{-3}E^2+\left(2C_2^2-C_1C_3\right)C_1^{-5}E^3+\cdots$$
$$=2s/ik_0-s^2/k_0^2+O\left(s^{2M+1}\right), \quad (3.19)$$

which results in vertical wavenumbers γ_M of the same order of accuracy in s as those obtained in (3.14). Apart from the Tappert PE, all of the vertical wavenumbers agree to at least $O(s^3)$, a somewhat unexpected but useful result.

In principle, with the reflection coefficient R specified, we are in a position to derive non-local boundary conditions for the inhomogeneous waveguide. Unfortunately, only in a few special cases can the inner integral g be carried out analytically. Specifically, these cases involve either the Tappert, the Claerbout, or the Exact vertical wavenumbers—it does not appear possible to proceed analytically when multiple-term regular or split-step Padé approximations are involved. In order to apply NLBC's to higher-order algorithms, we are faced either with performing the inner integral numerically [27, 31] or using some alternative approximations. Since γ_M^2 is accurate to second-order in s for $M\geq 1$, we are motivated to go the latter route and use an NLBC derived from a low-order expressions for the vertical wavenumber and then apply this boundary condition within the context of a high-order PE algorithm.

3.2 A Rough Free Surface

To derive the non-local boundary condition that represents the effects of a rough zero-mean Gaussian free surface at $z=0$, we start with the surface reflection coefficient, R_0. In the context of the Claerbout PE, R_0 is given by [3, p. 54]

$$R_0=-\exp\left[-2\sigma_0^2\gamma_1^2(0)\right], \quad (3.20)$$

where σ_0 is the *rms* surface roughness and the explicit dependence on s has been suppressed. Substituting (3.20) into (3.3) leads to the surface impedance,

$$G_0=\frac{i\rho_0}{\gamma_1(0)}\tanh\left[\sigma_0^2\gamma_1^2(0)\right], \quad (3.21)$$

where $\rho_0 = \rho(0)$. As it stands, G_0 cannot be inverted analytically in (3.4). For the low-angle energy that is expected to dominate long-range propagation, however, a tractable form can be obtained by retaining only the first term in the power series expansion of G_0, i.e.,

$$G_0 = i\rho_0\sigma_0^2\gamma_1(0) + O\left(\gamma_1^3\right). \tag{3.22}$$

Substituting (3.9) and (3.22) into (3.4) and manipulating the inner integrand leads to the approximate non-local rough-surface boundary condition in the form of a Neumann to Dirichlet map (NtD),

$$\begin{aligned}
&\psi(r,0) - ik_0\sigma_0^2\sqrt{\kappa_0}\,\psi_z(r,0) \\
&\quad = ik_0\sigma_0^2\sqrt{\kappa_0}\int_0^r \psi_z(r-t,0)\left(\frac{1}{2\pi i}\int_{\varepsilon-i\infty}^{\varepsilon+i\infty}\left[\sqrt{\frac{s-2ik_0\mu_0}{s-2ik_0}}-1\right]e^{st}ds\right)dt \\
&\quad = -k_0\sigma_0^2\sqrt{\kappa_0}\,\tau_0^-\int_0^r \psi_z(r-t,0)\exp(i\tau_0^+t)\mathcal{K}_+(\tau_0^-t)dt,
\end{aligned} \tag{3.23}$$

where we have defined $\kappa_0 = N_0^2 + 3$, $\kappa_0\mu_0 = N_0^2 - 1$, $\tau_0^\pm = k_0(1 \pm \mu_0)$, $N_0 = N(0)$, and introduced the kernel $\mathcal{K}_\pm(x) = J_0(x) \pm iJ_1(x)$. J_0, J_1 denote Bessel functions of the first kind. The inverse transform in (3.23) was evaluated analytically using the result tabulated in [37. p. 60. #561.0].

In contrast, replacing γ_1 with γ_0, a non-local rough-surface boundary condition for the Tappert PE can be derived in the form of the Dirichlet to Neumann (DtN) mapping,

$$\psi_z(r,0) = -\left(B_0/\sigma_0^2\right)\int_0^r \psi(r-t,0)\exp\left(ib_0t\right)\frac{dt}{\sqrt{t}}, \tag{3.24}$$

where $B_0 = \sqrt{i/(2\pi k_0)}$ and $b_0 = \frac{1}{2}\,k_0\kappa_0\mu_0$. A similar analysis for the Exact PE determines a non-local rough-surface boundary condition in the DtN form

$$\psi_z(r,0) = -\left(i/\sigma_0^2\right)\int_0^r \psi(r-t,0)\exp(-ik_0t)J_0\left(k_0N_0t\right)dt. \tag{3.25}$$

The non-local boundary conditions given in (3.23)–(3.25) approximate the effects of a rough zero-mean Gaussian free surface at $z = 0$. Because they are based on a low-order series expansion of the vertical wavenumbers for the Claerbout, Tappert and Exact PE's respectively, they are expected to be most accurate for lower-angle propagation found in shallow-water at long ranges. Each NLBC will be implemented later in the context of the higher-order split-step Padé PE algorithm.

3.3 Fluid Half-space

For completeness, we include in this section the non-local boundary conditions that represent the effects of a fluid half-space in $z > z_b$ (c.f. [27, 28, 29]). In this case, the NLBC's account for bottom losses due to the transmission of sound into the sea-bottom. A plane wave incident upon the interface from $z < z_b$ gives rise to a fluid/fluid reflection coefficient in the form

$$R_b = \frac{\gamma_1(z_b^-) - \left(\rho_b^-/\rho_b^+\right)\gamma_1(z_b^+)}{\gamma_1(z_b^-) + \left(\rho_b^-/\rho_b^+\right)\gamma_1(z_b^+)} \tag{3.26}$$

where $z_b^{\pm} = z_b \pm 0$, and $\rho_b^{\pm} = \rho(z_b^{\pm})$. In the Claerbout approximation, substituting (3.26) into (3.3) yields the impedance function

$$G_b = \frac{\rho_b^-}{i\gamma_1(z_b^-)} \frac{1+R_b}{1-R_b} \equiv \frac{\rho_b^+}{i\gamma_1(z_b^+)}. \tag{3.27}$$

Use of (3.27) in conjunction with (3.4) and (3.9) leads to a NtD boundary condition for a penetrable sea-bottom in the form (cf. the DtN form given in [28, Eq. (15)])

$$\begin{aligned} &\psi(r,z_b) + \frac{i(\rho_b^+/\rho_b^-)}{k_0\sqrt{\kappa_b}}\psi_z(r,z_b) \\ &\quad = -\frac{\tau_b^-(\rho_b^+/\rho_b^-)}{k_0\sqrt{\kappa_b}} \int_0^r \psi_z(r-t,z_b)\exp(i\tau_b^+ t)\,\mathcal{K}_-(\tau_b^- t)dt, \end{aligned} \tag{3.28}$$

where $\kappa_b = N_b^2 + 3$, $\kappa_b\mu_b = N_b^2 - 1$, $\tau_b^{\pm} = k_0(1 \pm \mu_b)$, and $N_b = N(z_b^+)$.

Similarly, the NtD condition for the Tappert PE is found to be

$$\psi(r,z_b) = -B_0(\rho_b^+/\rho_b^-)\int_0^r \psi_z(r-t,z_b)\exp(ib_b t)\,\frac{dt}{\sqrt{t}}, \tag{3.29}$$

where $b_b = \frac{1}{2}k_0\kappa_b/\mu_b$ while the NLBC corresponding to the Exact PE is

$$\psi(r,z_b) = -i(\rho_b^+/\rho_b^-)\int_0^r \psi_z(r-t,z_b)\exp(-ik_0 t)J_0(k_0 N_b t)\,dt. \tag{3.30}$$

The numerical procedures used to implement these NLBC's are presented in Appendix B.

3.4 Discussion

The Exact NLBC's in (3.25) and (3.30) are observed to depend on $J_0(k_0 N t)$ and appear to exhibit improper asymptotic behaviour (particularly for lossy media where N is complex). Our derivation of γ in (3.15) essentially required taking the square of (3.5) and thus corresponds to the vertical wavenumber associated with the Helmholtz equation. As a result, the Exact boundary condition incorporates a component associated with incoming waves, and has the potential for numerical instability when implemented within the context of a one-way algorithm. This aspect of the Exact NLBC will be alluded to in the numerical examples that follow.

In principle, approximate non-local boundary conditions could be derived for higher-order Padé and split-step Padé PE's using the same methodology described above, although numerical implementation would prove difficult. Instead, because of the similarity of the vertical wavenumbers (as functions of s) between all PE algorithms, we are motivated to use first-order Tappert and Claerbout NLBC's in conjunction with higher-order PE propagators. Our numerical results support this conjecture. Where appropriate (in a lossless waveguide or at a rough free surface) we show that high-order PE's combined with the Exact NLBC can also yield stable and accurate calculations.

4 Numerical Examples

An energy-conserving [13] split-step Padé code derived from a finite-difference PE formulation [29, 38] has been modified to accommodate each of six different NLBC's described above, i.e., (3.23)–(3.25) for the surface roughness and (3.28)–(3.30) for the fluid half-space. Three numerical examples are considered that demonstrate specific characteristics or properties of the PE fields generated using the various NLBC's. For the two range-independent test cases, reference solutions were obtained using SAFARI [39], which has the capability of allowing roughness (Gaussian statistics) at interfaces between homogeneous elastic layers [40]. Two-way COUPLE [41, 42] is used to provide the reference results for the ASA Wedge problem.

4.1 Example 1: Bucker waveguide

The Bucker waveguide [3, pp. 249–251] consists of a shallow ocean containing a bilinear sound speed profile $c(z) = 1498 + |120 - z|/60$ m s^{-1} and density 1 g cm^{-3} in $0 < z < 240$ m above a uniform fluid of sound speed 1505 m s^{-1} and density 2.1 g cm^{-3}, respectively. There is no intrinsic loss in this problem. Calculations are carried out at a frequency of 100 Hz for a source depth of 30 m and a receiver depth of 90 m. SAFARI and split-step Padé PE transmission losses ($-10 \log_{10} |p|^2$) versus range are compared in Fig. (1). The PE curve

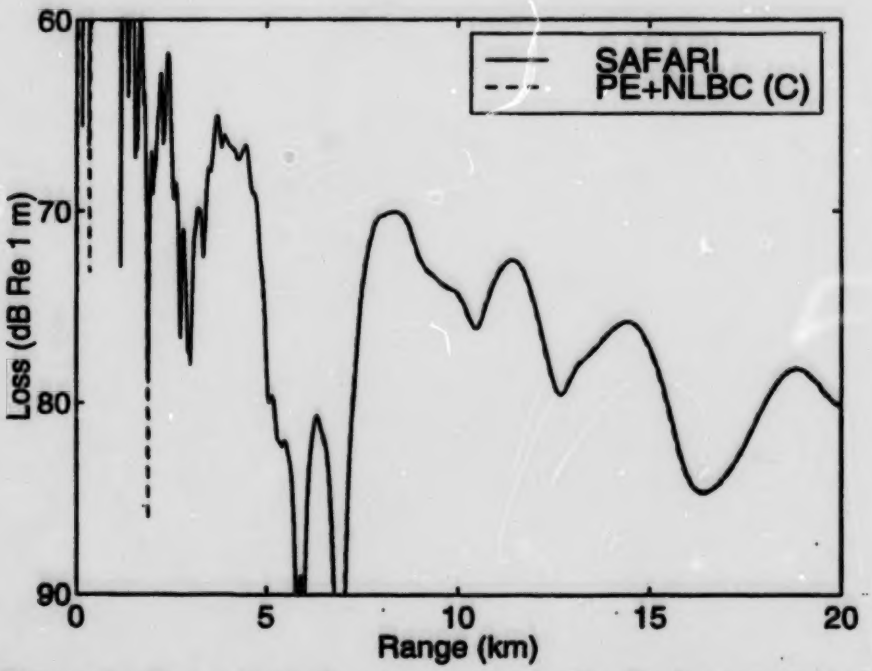

Figure 1: *Transmission loss comparison for the Bucker waveguide.*

was obtained using $M = 2$, $\Delta r = 10$ m, $\Delta z = 1$ m with the Claerbout (C) NLBC applied

along $z = 240$ m. The agreement is seen to be excellent. Corresponding results obtained with the Tappert (T) NLBC using $M = 2$, $\Delta r = 100$ m and the Exact (E) NLBC using $M = 3$, $\Delta r = 400$ m are compared to the SAFARI curve in Fig. (2). Although the range sampling is too large to resolve individual peaks at shorter ranges, the agreement at longer

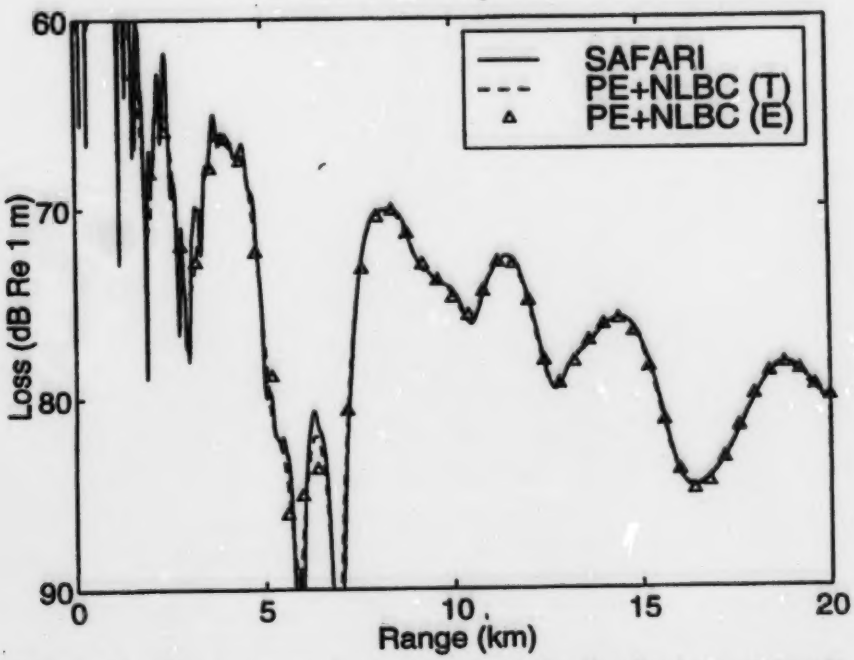

Figure 2: *Transmission loss comparison for the Bucker waveguide.*

ranges is excellent. The Bucker problem demonstrates, in principle, that the use of NLBC's does not compromise the efficiency of the split-step Padé algorithm, i.e., the ability to take large range steps. Although the Bucker problem is relatively benign in the sense that it involves narrow-angle propagation, it does show that each of the fluid half-space NLBC's can be incorporated within the context of a multi-term split-step Padé PE.

4.2 Example 2: Pekeris waveguide

Example 2 corresponds to the Pekeris waveguide introduced at a NORDA Workshop as test case 3 [24]. The region $0 < z < 100$ m contains a homogeneous fluid with sound speed 1500 m s^{-1} and density 1 g cm^{-3} that overlays a fluid half-space with constant sound speed, density and absorption of 1590 m s^{-1}, 1.2 g cm^{-3} and 0.5 dB λ^{-1}, respectively. The source and receiver depths are both equal to 50 m. The 250-Hz source frequency gives rise to 11 propagating modes in this waveguide. In addition to the original waveguide configuration, we consider a modified version obtained by adding an *rms* surface roughness of 4 m.

The SAFARI and PE transmission loss results shown in Fig. (3) and Fig. (4) compare the propagation for a smooth surface ($\sigma_0 = 0$ m) to that of a rough surface ($\sigma_0 = 4$ m)

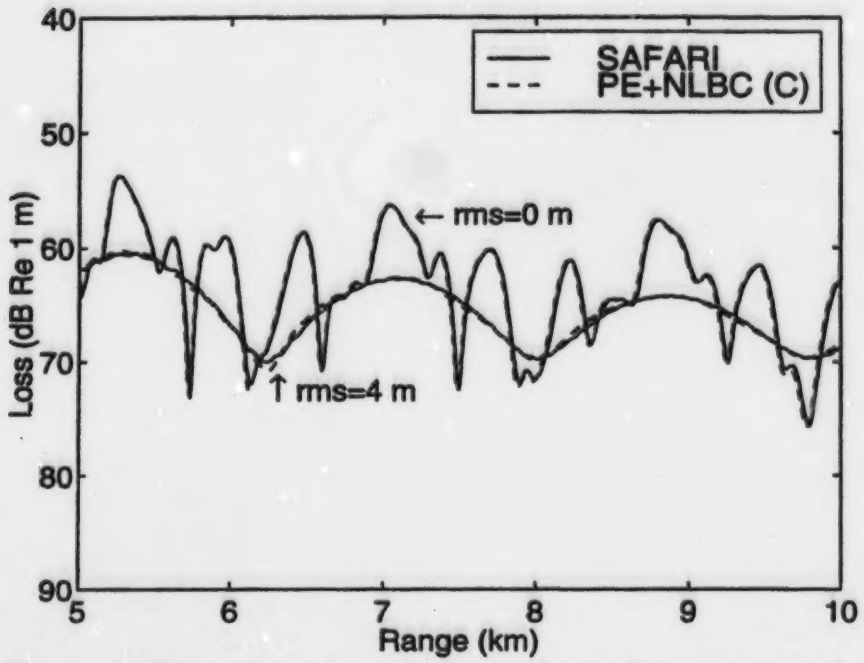

Figure 3: *Transmission loss comparison for the Pekeris waveguide.*

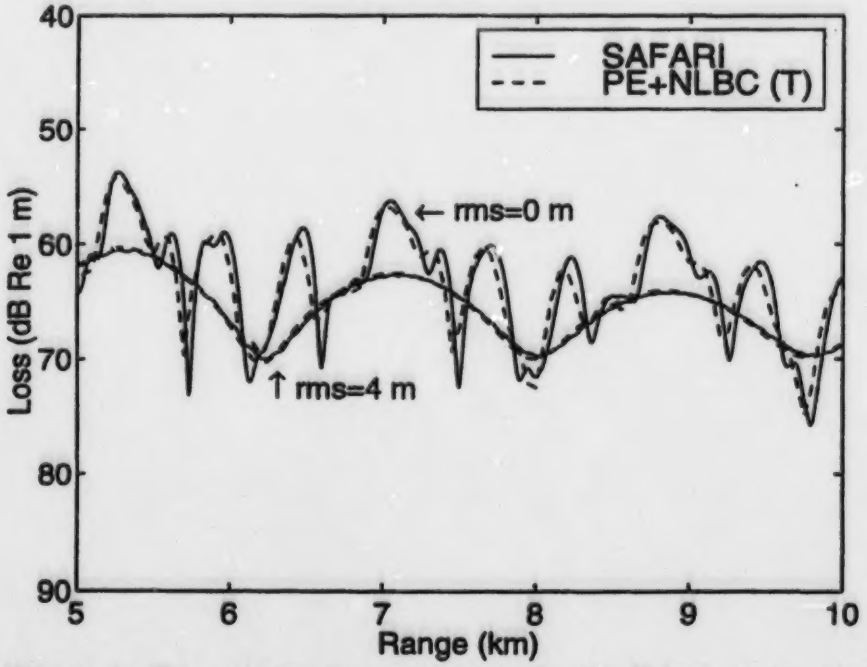

Figure 4: *Transmission loss comparison for the Pekeris waveguide.*

for the Pekeris waveguide. For the PE calculations in Fig. (3), we used a two-term Padé approximation ($M = 2$) and grid sizes $\Delta r = 5$ m, $\Delta z = 0.25$ m. The PE results for $\sigma_0 = 0$ m were obtained by applying Claerbout's (C) NLBC along $z = 100$ m. In contrast, the PE results for $\sigma_0 = 4$ m were obtained using NLBC's applied along *both* $z = 0$ m and $z = 100$ m. At this frequency, the 4-m *rms* surface roughness is observed to have a considerable effect on the far-field propagation. Due to the stripping of the higher-order modes, the transmission loss results are considerably smoother and the overall levels have increased by several dB. Similar agreement (not shown) is obtained with the Tappert NLBC.

Further PE calculations for this example were carried out using $M = 3$, $\Delta r = 50$ m. Although stable, the results shown in Fig. (4) obtained with Tappert's NLBC (T) applied top and bottom for this larger range step size are not as good as those shown in Fig. (3) and indicate a limitation on Δr for this problem. On the other hand, the Exact NLBC applied along $z = 100$ m was found to be unstable in this case for either value of Δr. We believe that this is due to the presence of loss in the lower half-space and the improper asymptotic behaviour of $J_0(k_0 N t)$. Moreover, the agreement obtained for the Claerbout NLBC using $M = 3$, $\Delta r = 50$ m is considerably worse than that for the Tappert NLBC. We attribute this decrease in accuracy to approximations inherent in our numerical integration procedure for integrals involving Bessel functions. For lossy media and high frequencies, our current numerical scheme for implementing this boundary condition precludes the capability for larger step sizes that are characteristic of split-step Padé methods.

4.3 Example 3: ASA Wedge

The ASA Wedge [42] is a shallow-water shoaling waveguide in which the water depth decreases from 200 m to 0 m over a range of 4 km. The homogeneous wedge has a sound speed of 1500 m s^{-1} and a density of 1 g cm^{-3}. The fluid bottom has a constant sound speed, density and absorption of 1700 m s^{-1}, 1.5 g cm^{-3} and 0.5 dB λ^{-1}, respectively. Calculations are carried out at 25 Hz for a source located at $r = 0$ km and $z = 100$ m. For this range-dependent problem, the non-local boundary conditions in (3.28)–(3.30) were applied at a depth of 202 m, just below the water/bottom interface at the range of the source and below any changes in material properties of the medium. Consequently, the NLBC's act solely to absorb downgoing energy in this problem. Curves of transmission loss versus range calculated for a receiver at a depth of 30 m are shown in Fig. (5) and Fig. (6). The reference results were obtained using the coupled mode code COUPLE [41, 42]. The energy-conserving PE curve for the Claerbout (C) NLBC, calculated using $\Delta r = 5$ m, $\Delta z = 1$ m, $M = 2$, agrees well with the COUPLE curve. PE results obtained using $M = 3$, $\Delta r = 50$ m for the Exact (E) and Tappert (T) non-local boundary conditions are shown in Fig. (6). For this larger range step-size, the observed departures from the coupled mode results are due to the range-dependence of the sloping interface and not to the numerical approximations used in evaluating the NLBC's, despite the fact that the bottom half-space is lossy. Evidently, at the low frequency and short ranges considered for this problem, the potential difficulties with computing Bessel functions of complex arguments is not an issue. This test case demonstrates that the NLBC's can be applied to range-dependent problems in a straightforward and efficient manner.

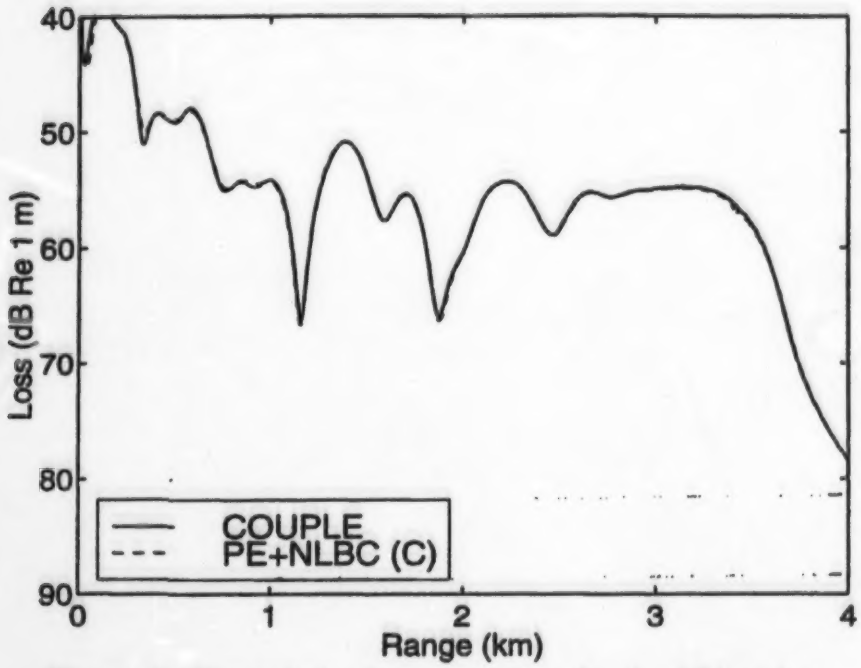

Figure 5: *Transmission loss comparison for the ASA wedge.*

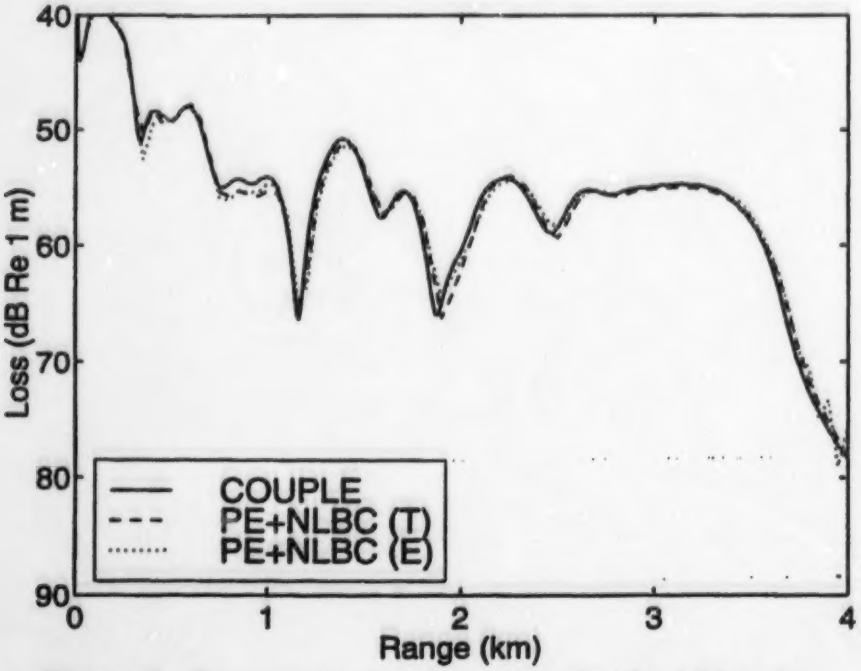

Figure 6: *Transmission loss comparison for the ASA wedge.*

5 Summary

An analysis of non-local boundary conditions applied in the context of multi-term higher-order PE algorithms has been carried out. Specifically, it has been shown that NLBC's derived on the basis of the boundary conditions satisfied by the total field also apply to the individual intermediate fields associated with higher-order solution procedures. Higher-order PE's can be combined with a formulation of the impedance boundary condition, based on the plane-wave reflection coefficient, to obtain non-local boundary conditions representing a wide range of waveguide layering and scattering effects. It was shown that the vertical wavenumber $\gamma_M(s)$ associated with an Mth-order PE field provides a useful framework for analyzing non-local boundary conditions. Since γ_M agrees with γ for the Exact PE to $O\left(s^{2M+1}\right)$, low-order PE approximations lead to vertical wavenumbers that approximate those corresponding to high-order algorithms. Consequently, higher-order NLBC's, which are difficult to implement numerically, can be replaced by non-local boundary conditions based on lower-order PE approximations and then used in conjunction with the higher-order propagators interior to the computational domain. For the special case of a rough surface characterized by Gaussian statistics, we imposed a low-angle condition to derive an approximate NLBC that can be easily implemented in higher-order PE's. Three examples involving rough sea surfaces and/or penetrable ocean bottoms were used to demonstate the implementation of non-local conditions in a multi-term, split-step Padé PE. For most examples, the NLBC's did not degrade the large range step capability of the split-step Padé algorithm.

References

1. A. Tolstoy, *Matched Field Processing in Underwater Acoustics* (World Scientific, Singapore, 1993).

2. M.J. Buckingham, Ocean-acoustic propagation models, *J. Acoustique* **3** (1992) 223–287.

3. F.B. Jensen, W.A. Kuperman, M.B. Porter and H. Schmidt, *Computational Ocean Acoustics* (AIP Press, New York, 1994).

4. F.D. Tappert and R.H. Hardin, Computer simulation of long-range ocean acoustic propagation using the parabolic equation method, in: *Proceedings of the 8th International Congress on Acoustics, Vol. 2* (Goldcrest, London, 1974) 452.

5. F.D. Tappert, The parabolic approximation method, in: J.B. Keller and J.S. Papadakis, eds., *Wave Propagation and Underwater Acoustics* (Springer, New York, 1977) 224–287.

6. D.J. Thomson and N.R. Chapman, A wide-angle split-step algorithm for the parabolic equation, *J. Acoust. Soc. Am.* **74** (1983) 1848–1854.

7. D. Lee and S.T. McDaniel, Ocean acoustic propagation by finite-difference methods, *Comput. Math. Appl.* **14** (1987) 305–423.

8. M.D. Collins, Higher-order, energy-conserving, two-way, and elastic parabolic equations, in: S.A. Chin-Bing, D.B. King, J.A. Davis and R.B. Evans, eds., *PE Workshop II: Proceedings of the Second Parabolic Equation Workshop* (US Government Printing Office. Washington, DC, 1993) 145–168.

9. M.D. Collins, R.J. Cederberg, D.B. King and S.A. Chin-Bing, Comparison of algorithms for solving parabolic wave equations, *J. Acoust. Soc. Am.* **100** (1996) 178–182.

10. A. Bamberger, B. Engquist, L. Halpern and P. Joly, Higher order paraxial wave equation approximations in heterogeneous media, *SIAM J. Appl. Math.* **48** (1988) 129–154.

11. M.D. Collins, Benchmark calculations for higher-order parabolic equations, *J. Acoust. Soc. Am.* **87** (1990) 1535–1538.

12. F.A. Milinazzo. C.A. Zala and G.H. Brooke, Rational square-root approximations for parabolic equation algorithms, *J. Acoust. Soc. Am.* **101** (1997) 760–766.

13. M.D. Collins and E.K. Westwood, A higher-order energy-conserving parabolic equation for range-dependent ocean depth, sound speed, and density, *J. Acoust. Soc. Am.* **89** (1991) 1068–1075.

14. M.D. Collins, The split-step Padé solution for the parabolic equation method, *J. Acoust. Soc. Am.* **93** (1993) 1736–1742.

15. M.D. Collins, A higher-order parabolic equation for wave propagation in an ocean overlying an elastic bottom, *J. Acoust. Soc. Am.* **86** (1989) 1459–1464.

16. B.T.R. Wetton and G.H. Brooke, One-way wave equations for seismoacoustic propagation in elastic waveguides, *J. Acoust. Soc. Am.* **87** (1990) 624–632.

17. M.D. Collins. Higher-Order Padé approximations for accurate and stable elastic parabolic equations with application to interface wave propagation, *J. Acoust. Soc. Am.* **89** (1991) 1050–1057.

18. M.D. Collins and R.B. Evans, A two-way parabolic equation for acoustic backscattering in the ocean, *J. Acoust. Soc. Am.* **91** (1992) 1357–1368.

19. G.H. Brooke and D.J. Thomson, A single-scatter formalism for improving PE calculations in range-dependent media, in: S.A. Chin-Bing, D.B. King, J.A. Davis and R.B. Evans, eds., *PE Workshop II: Proceedings of the Second Parabolic Equation Workshop* (US Government Printing Office, Washington, DC, 1993) 126–144.

20. M.D. Collins, A two-way parabolic equation for elastic media, *J. Acoust. Soc. Am.* **93** (1993) 1815–1825.

21. M.D. Collins, W.A. Kuperman and W.L. Siegmann, A parabolic equation for poroelastic media, *J. Acoust. Soc. Am.* **98** (1995) 1645–1656.

22. M.D. Collins. J.F. Lingevitch and W.L. Siegmann, Wave propagation in poro-acoustic media. *Wave Motion* **25** (1997) 265–272.

23. J.F. Lingevitch and M.D. Collins, Wave propagation in range-dependent poro-acoustic waveguides, *J. Acoust. Soc. Am.* **104** (1998) 783–790.

24. J.A. Davis, D. White, and R.C. Cavanagh, *NORDA Parabolic Equation Workshop, 31 March–3 April, 1981* Tech. Note 143, Naval Ocean Research and Development Activity, NSTL Station, MS (1982).

25. S.W. Marcus, A generalized impedance method for application of the parabolic approximation to underwater acoustics, *J. Acoust. Soc. Am.* **90** (1991) 391–398.

26. V.A. Baskakov and A.V. Popov, Implementation of transparent boundaries for numerical solution of the Schrodinger equation, *Wave Motion* **14** (1991) 121–128.

27. J.S. Papadakis, M.I. Taroudakis, P.J. Papadakis and B. Mayfield, A new method for a realistic treatment of the sea bottom in the parabolic approximation, *J. Acoust. Soc. Am.* **92** (1992) 2030–2038.

28. J.S. Papadakis, Exact, nonreflecting boundary conditions for parabolic-type approximations in underwater acoustics, *J. Comp. Acoust.* **2** (1994) 83–98.

29. D.J. Thomson and M.E. Mayfield, An exact radiation condition for use with the *a posteriori* PE method, *J. Comp. Acoust.* **2** (1994) 113–132.

30. T.W. Dawson, D.J. Thomson and G.H. Brooke, Non-local boundary conditions for acoustic PE predictions involving inhomogeneous layers, in: J.S. Papadakis, ed., *3rd European Conference on Underwater Acoustics* (FORTH-IACM, Heraklion, 1996) 183–188.

31. M.E. Mayfield and D.J. Thomson, An FFT-based non-local boundary condition for the parobolic equation, in: J.S. Papadakis, ed., *3rd European Conference on Underwater Acoustics* (FORTH-IACM, Heraklion, 1996) 237–242.

32. M.F. Levy. Transparent boundary conditions for parabolic equation solutions of radiowave propagation problems, *IEEE Trans. Antenn. Propag.* **45** (1997) 66–72.

33. D.J. Thomson and G.H. Brooke, Non-local boundary conditions for 1-way wave propagation, in: J.A. DeSanto, ed., *4th International Conference on Mathematical and Numerical Aspects of Wave Propgation* (SIAM, Golden, 1998) 348–352.

34. A. Arnold and M. Ehrhardt, Discrete transparent boundary conditions for wide angle parabolic equations in underwater acoustics, *J. Comp. Phys.* **145** (1998) 611–638.

35. D. Yevick and D.J. Thomson, Non-local boundary conditions for finite-difference PE solvers, *J. Acoust. Soc. Am.* **106** (1999) 143–150.

36. M. Abramowitz and A. Stegun, *Handbook of Mathematical Functions* (Dover, New York, 1965).

37. G.A. Campbell and R.M. Foster, *Fourier Integrals for Practical Applications* (D. Van Nostrand, New York, 1948).

38. D.J. Thomson, Wide-angle parabolic equation solutions to two range-dependent benchmark problems, *J. Acoust. Soc. Am.* **87** (1990) 1514–1520.

39. H. Schmidt, *SAFARI Seismo-Acoustic Fast field Algorithm for Range-Independent environments, User's Guide* Report SR–113, SACLANTCEN ASW Research Centre, San Bartolomeo, Italy (1988).

40. W.A. Kuperman and H. Schmidt, Rough surface elastic wave scattering in a horizontally stratified ocean, *J. Acoust. Soc. Am.* **79** (1986) 1767–1777.

41. R.B. Evans, A coupled mode solution for acoustic propagation in a waveguide with a stepwise depth variations of a penetrable bottom, *J. Acoust. Soc. Am.* **74** (1983) 188–195.

42. F.B. Jensen and C.M. Ferla, Numerical solution of range-dependent benchmark problems in ocean acoustics, *J. Acoust. Soc. Am.* **87** (1990) 1499–1510.

Appendices

A Intermediate PE Fields

In this appendix, we apply a modal analysis to the higher-order PE algorithms in order to determine the internal boundary conditions that are satisfied by the intermediate PE fields. Within a layered waveguide, the field satisfying (2.2) can be represented in terms of discrete modes as

$$\psi(r,z) = \sum_{n=1}^{\infty} c_n \phi_n(z) e^{ik_0 r\sqrt{\lambda_n}} \tag{A.1}$$

where the mode eigenfunctions ϕ_n are solutions of

$$\rho \frac{\partial}{\partial z}\left(\rho^{-1}\frac{\partial \phi_n}{\partial z}\right) + k_0^2\left[N^2 - \lambda_n\right]\phi_n = 0, \tag{A.2}$$

and satisfy the orthogonality relationship

$$\int_0^{z_B} \rho^{-1}(z)\phi_n(z)\phi_l(z)dz = \delta_{nl}. \tag{A.3}$$

Each mode also satisfies suitable external boundary conditions at $z = 0$ and $z = z_B$ (e.g., Dirichlet) and the internal continuity condition for the impedance,

$$\left.\frac{\rho\Psi}{\partial_z\Psi}\right|_{z_b-0} = \left.\frac{\rho\Psi}{\partial_z\Psi}\right|_{z_b+0}, \tag{A.4}$$

across an interface $z = z_b$. For the exact square-root operator $\sqrt{1+X}$, the eigenvalue λ_n defines the horizontal wavenumber k_n of the modes according to $k_n = \sqrt{\lambda_n}$. in which case (A.1) is recognized as the normal mode expansion of the Helmholtz equation (2.1). PE methods invoke approximations to the square-root so that $\sqrt{\lambda_n} \approx F(\lambda_n)$ so that the mode expansion (A.1) becomes

$$\psi(r,z) = \sum_{n=1}^{\infty} c_n \phi_n(z) e^{iF(\lambda_n)r}. \tag{A.5}$$

Typical single-term approximations to the square-root include $F_0 = \frac{1}{2}(1+\lambda_n)$ for the Tappert PE and $F_1 = (1+3\lambda_n)(3+\lambda_n)^{-1}$ for the Claerbout PE. In any case, (A.5) represents a well-known result for PE fields [16], that is, they have the same mode eigenfunctions as the normal modes of the Helmholtz equation but the PE modal wavenumbers differ by amounts that depend on the square-root approximation used.

To develop a modal representation for the split-step Padé PE, we proceed as follows. Using (2.4). we first write

$$\begin{aligned}\psi(r+\Delta r. z) &= \sum_{n=1}^{\infty} e^{i\delta\sqrt{\lambda_n}} c_n \phi_n(z) e^{ik_0 r\sqrt{\lambda_n}} \\ &= \sum_{n=1}^{\infty} e^{i\delta\sqrt{1+(\lambda_n-1)}} c_n \phi_n(z) e^{ik_0 r\sqrt{\lambda_n}}.\end{aligned} \tag{A.6}$$

and then use (2.10) with X replaced by $\lambda_n - 1$ to obtain

$$\psi(r+\Delta r,z) = \sum_{n=1}^{\infty}\left(1+\sum_{m=1}^{M}\frac{A_m(\lambda_n-1)}{1+B_m(\lambda_n-1)}\right)c_n\phi_n(z)e^{ik_0r\sqrt{\lambda_n}}$$
$$= \psi(r,z)+\sum_{m=1}^{M}\psi_m(r,z), \tag{A.7}$$

where we have set

$$\psi_m(r,z) = \sum_{n=1}^{\infty}\frac{A_m(\lambda_n-1)}{1+B_m(\lambda_n-1)}c_n\phi_n(z)e^{ik_0r\sqrt{\lambda_n}}. \tag{A.8}$$

Noting from (A.2) that

$$X\phi_n(z) = (\lambda_n-1)\phi_n(z), \tag{A.9}$$

it is apparent that ψ_m in (A.8) reduces to

$$\psi_m(r,z) = \sum_{n=1}^{\infty}\frac{A_mX}{1+B_mX}c_n\phi_n(z)e^{ik_0r\sqrt{\lambda_n}} \equiv \frac{A_mX}{1+B_mX}\psi(r,z). \tag{A.10}$$

Since the intermediate PE fields for the split-step Padé algorithm (and any high-order finite-difference PE method for that matter) can be written as a summation over the complete set of modes for the waveguide, they satisfy the same internal boundary conditions as the individual modes ϕ_n and therefore the total field ψ. As a result, the non-local boundary conditions that are derived for the single-term finite-difference PE's also apply to the intermediate fields associated with higher-order PE's.

B NLBC Implementation

To obtain suitable numerical implementations for the non-local boundary conditions, we start with (3.29) for the standard PE in the form

$$\psi(r) = B\int_0^t \psi_z(r-t)\exp(ibt)\frac{dt}{\sqrt{t}}, \tag{B.1}$$

where, to simplify notation, we have dropped the subscripts on B and b, and suppressed the dependence on z_b. Following the original approach of Papadakis [28. 29], the range interval $0 \rightarrow t$ is divided into J subintervals of width Δt to obtain

$$\psi(J\Delta t) = B\sum_{j=0}^{J-1} I_j, \tag{B.2}$$

where

$$I_j = \int_{j\Delta t}^{(j+1)\Delta t}\psi_z(J\Delta t-t)\exp(ibt)\frac{dt}{\sqrt{t}}. \tag{B.3}$$

Let us consider the contribution I_0 first. The singularity at $t=0$ can be subtracted out, i.e.,

$$I_0 = \int_0^{\Delta t}\psi_z(J\Delta t-t)\left(\frac{\exp(ibt)-1}{\sqrt{t}}+\frac{1}{\sqrt{t}}\right)dt. \tag{B.4}$$

If we assume that $\psi_z = \alpha_0 t + \beta_0$ over $0 < t < \Delta t$, then the second term integrates readily to yield

$$I_{02} = 2\sqrt{\Delta t}\left(\tfrac{2}{3}\psi_z(J\Delta t) + \tfrac{1}{3}\psi_z[(J-1)\Delta t]\right). \tag{B.5}$$

To evaluate the first term in (B.4), expand $\exp(ibt)$ in a Taylor series and integrate term by term to obtain

$$\begin{aligned} I_{01} &= \sum_{k=1}^{\infty} \frac{(ib)^k}{k!} \int_0^{\Delta t} \left(\alpha_0 t^{k+\frac{1}{2}} + \beta_0 t^{k-\frac{1}{2}}\right) dt \\ &= 2\sqrt{\Delta t}\left(\mathcal{A}_0 \psi_z(T\Delta t) + \mathcal{B}_0 \psi_z[(J-1)\Delta t]\right), \end{aligned} \tag{B.6}$$

where the coefficients $\mathcal{A}_0$ and $\mathcal{B}_0$ are given by

$$\mathcal{A}_0 = \sum_{k=0}^{\infty} \frac{(ib\Delta t)^k}{(2k+1)k!} - \mathcal{B}_0, \qquad \mathcal{B}_0 = \sum_{k=0}^{\infty} \frac{(ib\Delta t)^k}{(2k+3)k!}. \tag{B.7}$$

Combining the results in (B.5) and (B.6) yields

$$I_0 = 2\sqrt{\Delta t}\left\{\left(\tfrac{2}{3} + \mathcal{A}_0\right)\psi_z(J\Delta t) + \left(\tfrac{1}{3} + \mathcal{B}_0\right)\psi_z[(J-1)\Delta t]\right\}. \tag{B.8}$$

Since $1/\sqrt{t}$ decays slowly with t away from the origin, for $j > 0$, we set $h(t) = \psi_z(J\Delta t - t)/\sqrt{t}$ and assume $h(t) = \alpha_j t + \beta_j$ within each segment $j\Delta t < t < (j+1)\Delta t$. The coefficients α_j and β_j are given by

$$\alpha_j = (h_{j+1} - h_j)/\Delta t, \qquad \beta_j = (j+1)h_j - jh_{j+1} \tag{B.9}$$

where $h_j = h(j\Delta t)$. For this form of h, (B.3) reduces to

$$\begin{aligned} I_j &= \int_{j\Delta t}^{(j+1)\Delta t} (\alpha_j t + \beta_j)\exp(ibt)dt \\ &= \Delta t \exp(ibj\Delta t)\left(w_+ h_j + w_- h_{j+1}\exp(ib\Delta t)\right), \end{aligned} \tag{B.10}$$

where the weights $w_\pm$ are defined by

$$w_\pm = \frac{1 \pm ib\Delta t - \exp(\pm ib\Delta t)}{(b\Delta t)^2}. \tag{B.11}$$

Substituting for h_j in (B.10) yields

$$\sum_{j=1}^{J-1} I_j = 2\sqrt{\Delta t} \sum_{j=1}^{J} w_j \psi_z[(J-j)\Delta t] \frac{\exp(ibj\Delta t)}{2\sqrt{j}}, \tag{B.12}$$

where $w_1 = w_+$, $w_J = w_-$, and $w_j = w_- + w_+$ for $j = 2, \ldots, J-1$. In the limit as $b\Delta t \to 0$, the w_j reduce to the weights for the Trapezoid Rule. Substituting (B.8) and (B.10) into (B.2) and re-arranging gives

$$\psi_z(J\Delta t) = G_0 \psi(J\Delta t) - \sum_{j=1}^{J} w_j G_j \psi_z[(J-j)\Delta t]. \tag{B.13}$$

where $G_0 = \left[2B\sqrt{\Delta t}\left(\frac{2}{3} + \mathcal{A}_0\right)\right]^{-1}$, $G_j = \frac{1}{2}\left(\frac{2}{3} + \mathcal{A}_0\right)^{-1} \exp(ibj\Delta t)/\sqrt{j}$, and we have modified w_1 to be $w_1 = w_+ + 2\left(\frac{1}{3} + \mathcal{B}_0\right)\exp(-ib\Delta t)$. Next, we assume that the first-order differential equation in (B.13) holds within $z_b - \Delta z < z < z_b$ and integrate from $z_b - \Delta z$ to z_b. Setting $E(x) = \exp(G_0 x)$, the NLBC for the Tappert PE can be evaluated approximately as

$$\begin{aligned}
&\psi(J\Delta t, z_b) - E(\Delta z)\psi(J\Delta t, z_b - \Delta z) \\
&\quad = -\sum_{j=1}^{J-1} w_j G_j \int_{z_b-\Delta z}^{z_b} \psi_\zeta[(J-j)\Delta t, \zeta] E(\zeta - z_b)\, d\zeta \\
&\quad \approx -E(\tfrac{1}{2}\Delta z) \sum_{j=1}^{J-1} w_j G_j \Delta\psi[(J-j)\Delta t, z_b],
\end{aligned} \tag{B.14}$$

where $\Delta\psi[(J-j)\Delta t, z_b] = \psi[(J-j)\Delta t, z_b] - \psi[(J-j)\Delta t, z_b - \Delta z]$. With slight modifications, (B.14) can be adapted to evaluate the rough-surface boundary condition for the Tappert PE given in (3.24).

The NLBC's derived from the Claerbout PE are algebraically more cumbersome. We discretize (3.23) for the rough surface to obtain

$$\psi(J\Delta t) + iB^*\psi_x(J\Delta t) = \tau_0^- B^* \sum_{j=0}^{J-1} I_j^*, \tag{B.15}$$

where $B^* = -k_0\sigma_0^2\sqrt{\kappa_0}$ and

$$I_j^* = \int_{j\Delta t}^{(j+1)\Delta t} \psi_x(J\Delta t - t)\exp(i\tau_0^+ t)\mathcal{K}_+(\tau_0^- t)\, dt. \tag{B.16}$$

Since $\mathcal{K}_+(\tau_0^- t) = J_0(\tau_0^- t) + iJ_1(\tau_0^- t)$, we note that as $t \to \infty$,

$$\exp(i\tau_0^+ t)\mathcal{K}_+(\tau_0^- t) \sim \sqrt{2i/(\pi\tau_0^- t)}\exp(2ik_0\mu_0 t), \tag{B.17}$$

from which it is clear that I_j^* can be evaluated in a way similar to I_j for the standard NLBC, provided j is sufficiently large.

Alternatively, we note that by choosing c_0 so that $N_0 = 1$, then $\tau_0^\pm = k_0$. Setting $h^*(t) = \psi_x(J\Delta t - t)$, we let $h^*(t) = \alpha_j^* t + \beta_j^*$ within $j\Delta t < t < (j+1)\Delta t$. The coefficients α_j^* and β_j^* are given by

$$\alpha_j^* = (h_{j+1}^* - h_j^*)/\Delta t, \qquad \beta_j^* = (j+1)h_j^* - jh_{j+1}^*, \tag{B.18}$$

where $h_j^* = h^*(j\Delta t)$. With this form of h^*, we can use [36, 11.3.9] and integration by parts to evaluate (B.16) as

$$\begin{aligned}
I_j^* &= \int_{j\Delta t}^{(j+1)\Delta t} (\alpha_j^* t + \beta_j^*)\exp(ik_0 t)[J_0(k_0 t) + iJ_1(k_0 t)]\, dt \\
&= ik_0^{-1}(w_j^- h_j^* + w_j^+ h_{j+1}^*)\exp(ix_j),
\end{aligned} \tag{B.19}$$

where we set $x_j = jk_0\Delta t$. The weights $w_j^\pm$ are given by $w_j^- = J_0(x_j) + \mathcal{W}_j$ and $w_j^+ = J_0(x_{j+1})\exp(ik_0\Delta t) - \mathcal{W}_j$, respectively, where $\mathcal{W}_j$ is defined by

$$\mathcal{W}_j = j\mathcal{K}_-(x_j) - (j+1)\mathcal{K}_-(x_{j+1})\exp(ik_0\Delta t). \tag{B.20}$$

Substituting for h_j^* in (B.19) yields

$$\sum_{j=0}^{J-1} I_j^* = (i/k_0) \sum_{j=0}^{J} w_j^* \psi_z[(J-j)\Delta t] \exp(ix_j), \tag{B.21}$$

where $w_0^* = w_0^-$, $w_j^* = w_{j-1}^+$, and $w_j^* = w_{j-1}^+ \exp(-ik_0\Delta t) + w_j^-$ otherwise.

Combining (B.16) and (B.21) and re-arranging produces the result

$$\psi_z(J\Delta t) = G_0^* \psi(J\Delta t) - \sum_{j=1}^{J} G_j^* w_j^* \psi_z[(J-j)\Delta t], \tag{B.22}$$

where $G_0^* = [iB^*(1 - w_0^*)]^{-1}$ and $G_j^* = (1 - w_0^*)^{-1} \exp(ix_j)$. Setting $E^*(x) = \exp(G_0^* x)$, and assuming that (B.22) holds in the region $0 < z < \Delta z$, it can be integrated to yield the rough-surface NLBC for the Claerbout PE in the form

$$\begin{aligned} &\psi(J\Delta t, 0) - E^*(\Delta z)\psi(J\Delta t, \Delta z) \\ &\quad = -\sum_{j=1}^{J-1} w_j^* G_j^* \int_{\Delta z}^{0} \psi_\zeta[(J-j)\Delta t, \zeta] E^*(\zeta - z_b) d\zeta \\ &\quad \approx E^*(\tfrac{1}{2}\Delta z) \sum_{j=1}^{J} G_j^* w_j^* \Delta\psi[(J-j)\Delta t, 0], \end{aligned} \tag{B.23}$$

where $\Delta\psi[(J-j)\Delta t, 0] = \psi[(J-j)\Delta t, \Delta z] - \psi[(J-j)\Delta t, 0]$. With some modifications, (B.23) can be adapted for use with the Claerbout NLBC for a fluid bottom given in (3.28). The main difference is that one doesn't usually have the freedom to choose c_0 as conveniently as in the case of the rough surface, and as a result, an extra exponential factor has to be removed from the integrand to obtain an integrable form like (B.19) (e.g., see [28]).

UNCLASSIFIED
SECURITY CLASSIFICATION OF FORM
(highest classification of Title, Abstract, Keywords)

DOCUMENT CONTROL DATA

(Security classification of title, body of abstract and indexing annotation must be entered when the overall document is classified)

1. ORIGINATOR (the name and address of the organization preparing the document. Organizations for whom the document was prepared, e.g. Establishment sponsoring a contractor's report, or tasking agency, are entered in section 8.)

Defence Research Establishment Atlantic
PO Box 1012
Dartmouth, Nova Scotia, Canada B2Y 3Z7

2. SECURITY CLASSIFICATION (overall security classification of the document including special warning terms if applicable).

UNCLASSIFIED

3. TITLE (the complete document title as indicated on the title page. Its classification should be indicated by the appropriate abbreviation (S,C,R or U) in parentheses after the title).

Non-local boundary conditions for high-order PE models with application to scattering from a rough surface (U)

4. AUTHORS (Last name, first name, middle initial. If military, show rank, e.g. Doe, Maj. John E.)

Brooke, G.H. (Integrated Performance Decisions, Inc.) and Thomson, D.J.

5. DATE OF PUBLICATION (month and year of publication of document)	6a. NO .OF PAGES (total containing information Include Annexes, Appendices, etc).	6b. NO. OF REFS (total cited in document)
August 1999	28 (approx.)	42

7. DESCRIPTIVE NOTES (the category of the document, e.g. technical report, technical note or memorandum. If appropriate, enter the type of report, e.g. interim, progress, summary, annual or final. Give the inclusive dates when a specific reporting period is covered).

TECHNICAL MEMORANDUM

8. SPONSORING ACTIVITY (the name of the department project office or laboratory sponsoring the research and development. Include address).

Defence Research Establishment Atlantic

9a. PROJECT OR GRANT NO. (if appropriate, the applicable research and development project or grant number under which the document was written. Please specify whether project or grant).	9b. CONTRACT NO. (if appropriate, the applicable number under which the document was written).
1cc15	

10a ORIGINATOR'S DOCUMENT NUMBER (the official document number by which the document is identified by the originating activity. This number must be unique to this document.)	10b OTHER DOCUMENT NOs. (Any other numbers which may be assigned this document either by the originator or by the sponsor.)
DREA TM 1999-121	

11. DOCUMENT AVAILABILITY (any limitations on further dissemination of the document, other than those imposed by security classification)

(X) Unlimited distribution
( ) Defence departments and defence contractors; further distribution only as approved
( ) Defence departments and Canadian defence contractors; further distribution only as approved
( ) Government departments and agencies; further distribution only as approved
( ) Defence departments; further distribution only as approved
( ) Other (please specify):

12. DOCUMENT ANNOUNCEMENT (any limitation to the bibliographic announcement of this document. This will normally correspond to the Document Availability (11). However, where further distribution (beyond the audience specified in (11) is possible, a wider announcement audience may be selected).

Unlimited

UNCLASSIFIED
SECURITY CLASSIFICATION OF FORM

13. ABSTRACT (a brief and factual summary of the document. It may also appear elsewhere in the body of the document itself. It is highly desirable that the abstract of classified documents be unclassified. Each paragraph of the abstract shall begin with an indication of the security classification of the information in the paragraph (unless the document itself is unclassified) represented as (S), (C), (R), or (U). It is not necessary to include here abstracts in both official languages unless the text is bilingual).

Numerical PE (parabolic equation) solvers for underwater sound propagation usually approximate the subbottom radiation condition by appending an absorbing layer to the computational mesh. An alternative procedure uses a non-local boundary condition (NLBC) applied along (or below) the sea-bottom interface that exactly transforms the semi-infinite PE configuration into an equivalent bounded domain. In this report, we analyze non-local boundary conditions that are expressed in terms of plane-wave reflection coefficients and describe their numerical implementation in the context of higher-order Padé-based PE algorithms. In particular, we develop non-local boundary conditions to account for the coherent losses due to scattering by a statistically-rough sea surface. Several numerical examples are presented to illustrate the numerical implementation of NLBC's for higher-order PE's.

14. KEYWORDS, DESCRIPTORS or IDENTIFIERS (technically meaningful terms or short phrases that characterize a document and could be helpful in cataloguing the document. They should be selected so that no security classification is required. Identifiers, such as equipment model designation, trade name, military project code name, geographic location may also be included. If possible keywords should be selected from a published thesaurus. e.g. Thesaurus of Engineering and Scientific Terms (TEST) and that thesaurus-identified. If it not possible to select indexing terms which are Unclassified, the classification of each should be indicated as with the title).

parabolic equation (PE)
underwater sound propagation
radiation condition
absorbing layer
non-local boundary condition (NLBC)
plane-waves
reflection coefficients
Padé approximants
surface roughness
coherent losses
numerical implementation